Impact of Substrate and Bending Angle on the Performance of Microwave PCB Sensors for Permittivity Measurements

Sara Blazquez-Bello[a], Yolanda Campos-Roca[a,1], Axel Bangert[b], Carl Sandhagen[b]

[a] *Escuela Politécnica, Department of Computer and Communication Technologies, University of Extremadura, Spain.*
[b] *Microwave Electronics Lab, University of Kassel, Germany.*

Abstract

A design topology for a microwave planar permittivity sensor focused on manufacturing simplicity is proposed. Its operation is based on the first-notch frequency of the reflection parameter. The impacts of substrate and bending angle on the performance of this type of sensor are comparatively analyzed. Three flexible substrates are considered in comparison to three rigid ones. By full-wave electromagnetic analysis, the sensors have been simulated in contact to a material under test with a relative permittivity ranging between 1 and 20. The resulting shifts in the first-notch frequency show the potential of flexible environmentally-friendly substrates, such as liquid crystal polymer and paper, for the development of the sensors. In the flexible cases, the bending angles have been varied from 0 to 120°, producing deviations in S_{11} first-notch frequency of 0.4 to 4.7%. The simulation methodology is validated by experimental characterization of a prototype on Rogers 4003C laminate.

Keywords: Nondestructive evaluation, permittivity measurement, printed circuit board (PCB), microwave sensors, green electronics, flexible electronics.

[1]Corresponding author: Escuela Politécnica, Avenida de las Letras, s/n, 10003 Cáceres (Spain). E-mail address: ycampos@unex.es (Y. Campos-Roca).

1. Introduction

Dielectric characterization of materials has applications in multiple areas including, but not limited to, biomedical sensing [1], agriculture [2], food industry [3], civil engineering [4] or environmental monitoring [5, 6]. A common goal in some of these application fields is detection of moisture content [7], but other factors can be related to the permittivity of materials, such as chemical composition or physical structure.

In comparison to other microwave sensors that allow to perform permittivity measurements, planar resonators manufactured in a printed circuit board (PCB) technology show important advantages, such as small size and low fabrication cost. They can be used as measurement probes together with laboratory equipment (such as a network analyzer) [8, 9] or they can be integrated into an autonomous prototype to build a system-on-chip solution [10, 11] for an Internet-of-Things (IoT) application.

A variety of design concepts have been proposed to develop microwave planar sensors for permittivity measurements. It is common that they are based on ring resonators [12], split-ring resonators (SRR) [13, 14, 15] or complementary split-ring resonators (CSRR) [8]. The performance can be enhanced by using different techniques. For example, in [9], a ring resonator is surrounded by electromagnetic (EM) bandgap structures. [16] presents a different design concept based on a narrow bandpass microstrip filter with a differential structure.

For some applications, the geometrical shape of the material under test (MUT) is not flat and, therefore, it is convenient that the sensor can be bent for a better adaptation to its shape. For example, in the context of structural health monitoring, a potential application would be the assessment of physical condition of timber structures. These structures may be, for example, columns of cylindrical geometry which would require a flexible sensor. In [17], a flexible microwave sensor based on an SRR is presented for early detection of breaches in pipeline coatings. Very recent examples of flexible sensors are [18], based on CSRRs on Rogers ceramic-filled polytetrafluoroethylene laminates, [19], based

on a complementary spiral resonator on a polyethylene terephthalate substrate, and [20], based on an array of SRRs on Rogers Ultralam 3850 substrate mounted on a kirigami sheet. These examples have been manufactured by using subtractive techniques.

Apart from high performance, two important aspects that should be taken into account to develop sensors are sustainability and cost. On the one hand, cost is often the limiting factor for a microwave sensor to achieve industrial interest; on the other hand, eco-friendly solutions are necessary to minimize electronic waste that causes environmental degradation. In contrast to conventional subtractive manufacturing, additive manufacturing techniques such as inkjet printing are worth being considered to address these challenges.

Inkjet printing can be performed either with highly specialized and expensive equipment such as the FUJIFILM Dimatix DMP-2850 [21] or with an office printer (for example, Brother Inc. MFC-430W [22]). The second solution is very affordable, however, manufacturing constraints must be taken into account, so that only designs tolerant to these issues can be addressed. Taking the comparison between measurements and simulations as the reference, [23] obtained good agreement with two coplanar antenna designs operating at 1.82 and 2.45 GHz. Their layout geometries included 0.3 mm-wide gaps in the conductive layer. The printer was a low-cost Epson Stylus photo 1500W. [24, 25] are other examples of flexible antennas manufactured with low-cost printers on paper substrates. In these two cases, the designs did not include fine geometrical details. Concerning microwave resonator-based sensors, in [26], the measured performance of a modified SRR realized with Brother MFC-J430W printer on paper substrate is compared with simulations. The design used a 0.5 mm-wide gap in the conductive layer. The agreement between measurement and simulations showed some discrepancies, that may come from manufacturing tolerances.

Another relevant issue related to the development of flexible microwave circuits is the impact of bending on the performance. In [27], the effects of bending on the performances of printed microstrip transmission lines and power inductors are shown. These components were manufactured by chemical etching on

Kapton substrates. [28] investigates the impact of bending on SRRs based on elastomeric substrates manufactured by photolithography.

The idea behind this work was to propose a design topology for a permittivity sensor that can be considered also in the case of inkjet printing using low-cost equipment. The strategy lines up with the aforementioned antenna designs [24, 25], because the aim was to avoid critical elements in the geometry.

Based on the same design topology, different choices of substrates and manufacturing techniques for the development of permittivity sensors are comparatively analyzed through the use of three-dimensional (3D) full-wave EM simulations. Mechanically flexible substrates have been considered in comparison to rigid laminates, including liquid crystal polymer (LCP) and paper as sustainable options. One of the pursued goals was to examine to which extent the substrate has an impact on sensor performance, including in this investigation the impact of bending in the case of flexible substrates. More specifically, it was intended to check if a PCB microwave sensor, implemented on a low-cost paper substrate, could be useful despite the high dielectric loss of this substrate.

To validate the simulation methodology, a prototype test structure has been manufactured on a Rogers 4003C (RO4003C) laminate. The structure has been measured in air and in contact with samples of dielectric materials with low permittivity tolerance.

The main novel aspect of this work is the comparative analysis of an easy-to-manufacture sensor design concept for permittivity measurements on different rigid and flexible substrates. To the authors' best knowledge, this type of analysis has not been published before.

The structure of the paper is as follows. Section 2 summarizes the main features of the substrates. Next, Section 3 explains the design of the sensors, simulation methodology and experimental validation of a manufactured prototype in air. Section 4 analyzes the impact of rigid and flexible substrates on the performance of a flat permittivity sensor. This section includes an experimental validation of the RO4003C prototype in contact to common plastic MUTs. The impact of bending on sensor performance is covered in Section 5. A discussion

about the obtained results is presented in Section 6. The paper ends up with a conclusion (Section 7) and the main references.

2. Substrates and manufacturing techniques

Conventional manufacturing of RF and microwave PCBs is based on subtractive techniques, mainly chemical etching or mechanical milling, that remove areas of copper from a rigid copper-clad sheet. Later, laser etching emerged as an advantageous alternative providing high precision and speed for a low number of produced items. Among the wide variety of high-frequency laminates, three common commercially available types of substrates have been considered in this work: FR4, RO4003C and I-Tera MT RF. Their relevant characteristics are summarized in Table 1.

Table 1: Characteristic parameters of rigid laminates.

Substrate	FR4	RO4003C	I-Tera
Relative permittivity	4.70[†]	3.55[‡]	3.38
Dielectric thickness (mm)	1.600	0.813	0.508
Loss tangent (tan δ)	0.0140	0.0027	0.0028
Frequency (GHz)[§]	10	10	10
Metal thickness (μm)	18	18	18

For the aforementioned reasons, flexible substrates are currently receiving an increasing attention. Although subtractive techniques can also be applied to the flexible laminates considered, additive manufacturing (in particular, inkjet printing) constitutes a more recent technology which allows to reduce the amount of waste. Most examples of this manufacturing technique in the scientific literature are related to antennas [29, 30, 31]. There is a variety of inks that can be used, generally based on silver nanoparticles, although copper-based inks

[†] Value used in the simulations, tolerance of at least 4.35 to 4.8

[‡] Value for design, 3.38 ± 0.05 for material

[§] Frequency at which the manufacturer specifies permittivity and tan δ

are also available. All simulations on flexible substrates are based on parameter values corresponding to inkjet printing with silver nanoparticle ink.

Three types of flexible substrates have been considered: DuPont Kapton500HN [32], Ultralam 3850 LCP [33] from Rogers Corporation and two types of photographic paper, commercialized by Kodak [34] and Mitsubishi [35]. All the parameter values for the dielectric substrates are summarized in Table 2.

Table 2: Characteristic parameters of flexible substrates.

Substrate	Ultralam 3850-LCP	Kapton 500 HN	Misubishi photo-paper	Kodak photo-paper
Relative permittivity	2.9	3.5	2.9	2.8
Dielectric thickness (mm)	0.100	0.125	0.230	0.230
Loss tangent (tan δ)	0.0025	0.0026	0.08	0.055
Frequency (GHz)[¶]	10	1	24	1
Metal thickness (μm)	2.5	2.5	2.5	2.5

Concerning sustainability, LCP is a recyclable substrate and paper is one of the most environmentally-friendly materials. Another advantage of paper is its low cost. Examples of RF components based on paper substrates can be found in [36].

Electrical conductivity of inkjet printed traces has been assessed in the scientific literature. This conductivity is lower than that of the bulk material and depends on several factors, such as the specific printing process, the number of the printed passes and resulting thickness of the traces and the kind of substrate. A typical reference conductivity value for sintered silver ink is 2×10^7 S/m [37], for inkjet technologies using different sintering techniques.

[¶]Frequency at which the manufacturer specifies permittivity and tan δ

3. Structure design, simulation methodology and experimental validation in air

Direct-coupled microstrip resonators with low quality (Q) factor, operated in reflection mode, have been designed based on the different rigid and flexible dielectric substrates. The goal was to investigate the impact of substrate and bending angle (in the flexible case) on the performance of this structure as a permittivity sensor. The work is based on the principle that effective permittivity will change if a dielectric MUT is placed in the proximity of the sensor, resulting into a shift of the specific frequency. Therefore, the permittivity of the MUT can be estimated from the measured reflection coefficient.

3.1. Structure design

A permittivity sensor based on a microstrip resonator can be operated in transmission or reflection modes. Also, different design geometries are possible. In this case, layout constraints were imposed by taking low-cost manufacturing techniques into account. The idea was that the design was easy to realize so that it could be implemented using conventional inkjet printers. It was decided to avoid narrow gaps or slots, since there is not sufficient evidence about the performance of these elements when they are manufactured using low-cost printers (see Section 1).

The proposed design concept operates in reflection mode and is fed with microstrip transmission lines. Fig. 1 shows the 3D model of the sensor structure, with an MUT placed in contact with its surface. The main geometrical parameters, for the different substrates, are given in Table 3. w is the line width for a characteristic impedance of 50 Ω. The total length of the sensor is L_{PCB}. Each of the parallel-connected transmission lines between the two T-junctions has a length L. Since these two lines form a ring shape, the dimension D (diameter) can be easily calculated.

The structure resembles a ring resonator, but it is direct coupled and operated in reflection-mode. L is equal to half the guided wavelength ($\lambda/2$) at

the considered operation frequency. This length does not change the impedance (100 Ω at the parallel ports of both T-junctions, 50 Ω at the non-symmetrical ports). Therefore, it creates a notch in the reflection parameter S_{11} at this frequency. The presence of the MUT modifies the wave velocities in the transmission lines, shifting the frequency at which the electrical lengths are $\lambda/2$. This shift is related to the MUT permittivity and can be used to measure it. Since it is based on reflection, an additional advantage is that one-port measurements would be sufficient if the second port of the sensor is terminated by a 50 Ω load.

The operation frequency has been selected taking cost and size into account. In an IoT context of application, the sensor will operate autonomously. Therefore, additional circuits on the PCB will be necessary to perform the signal generation and readout. The cost of these circuits would increase with frequency. Also, paper substrates are very cost-efficient but they are lossy and their losses increase with frequency. On the other hand, the lower the frequency the bigger the size of the sensor. 1 GHz was a good compromise solution taking price and size into account. The size is calculated as $L_{PCB} \times (D + w)$ and it depends on the substrate, being the biggest size of 162.95×63.78 mm^2 (for Kodak photo-paper).

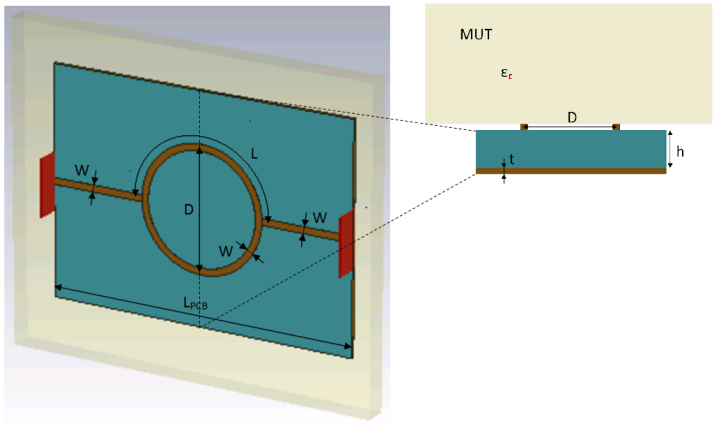

Figure 1: 3D model of an MUT (plotted using the transparent option) placed on the resonator and cross-sectional view at the middle length of the sensor. Dimensions given in Table 3.

Table 3: Dimensions of the planar microstrip sensors.

Substrate	w (mm)	L (mm)	L_{PCB} (mm)
FR4	3.00	82.27	137.60
RO4003C	1.83	92.02	152.37
I-Tera	1.15	91.97	151.60
Ultralam 3850-LCP	0.25	97.83	160.29
Kapton 500 HN	0.29	92.39	151.42
Misubishi paper	0.53	91.90	150.87
Kodak paper	0.60	99.25	162.95

3.2. EM simulation methodology and experimental validation in air

The sensors based on the different laminates were modeled via the 3D EM simulation software CST Microwave Studio. Simulations were run with the frequency domain solver.

In the case of sensors on flexible substrates, the conductive layers have been modeled using a conductivity value of 2×10^7 S/m, as explained in Section 2, to consider inkjet printing manufacturing.

The relative permittivity and loss tangent values of the dielectric substrates are defined by the manufacturer at the frequencies specified in Table I and Table II. CST includes a built-in Debye first-order model that has been used to simulate frequency dispersion for all dielectric materials. In the case of RO4003C substrate, the dielectric material is already pre-defined in CST and has been used.

For validation purposes, an experimental prototype has been manufactured on RO4003C substrate by using the available manufacturing technique (subtractive). This resonator prototype is shown in Figure 2. Figure 3 shows the comparison between simulated and measured S_{11} parameter versus frequency. S-parameter measurements have been obtained by means of a vector network analyzer. As it can be observed, a good agreement has been obtained.

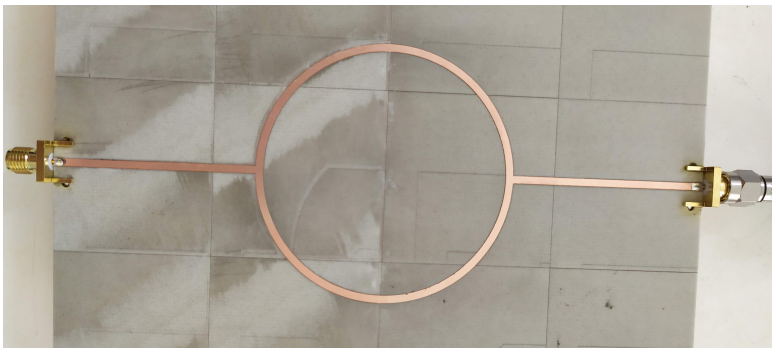

Figure 2: Photograph of the RO4003C PCB sensor.

4. Impact of substrate on permittivity sensor performance

To investigate the impact of substrate on the performance of the proposed sensor, first, full-wave simulations with lossless MUTs are considered. Subsequently, an experimental validation of the RO4003C prototype is presented, in which different low-loss MUTs (more concretely, plastic materials) are characterized. Finally, the impact of MUT losses on sensor performance is shown through a simulation example in the context of soil moisture sensing.

4.1. Substrate-dependent analysis based on 3D simulations with lossless MUTs

Simulations have been performed after placing a block of dielectric material or MUT on the resonator, as shown in Fig. 1. Substrate losses have been taken into account. The MUT is assumed to be lossless and its relative permittivity ϵ_r is varied within a wide range (from 1 to 20), that would cover a variety of applications. For example, for an application related to soil moisture measurement, ϵ_r may experiment variations between 4 and 20 when the soil changes from a dry condition up to a moisture content of 28.6% at 1.88 GHz, as reported in [38]. Another example in the context of structural health is assessment of physical condition of timber structures. It may involve variations of ϵ_r in the 2-15 range at 1.26 GHz due to volumetric moisture content variations from 0 to 60% [39].

Figs. 4 and 5 show simulated S_{11} parameters as a function of frequency for the sensors on different rigid and flexible substrates, respectively, with the MUT.

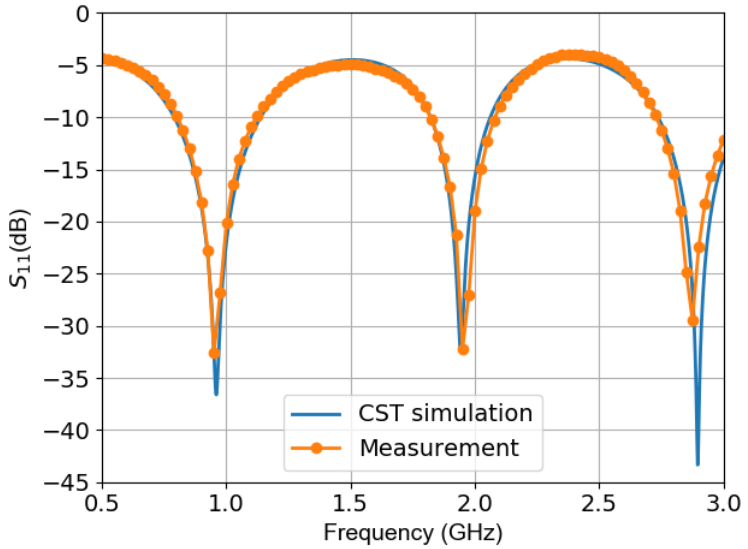

Figure 3: Comparison between simulation and measurement based on RO4003C substrate.

The first-notch frequency depends on ϵ_r. Fig. 6 shows the relative variation of this notch frequency when ϵ_r is increased from 1 to 20. This variation is calculated as the difference between the resonance frequency obtained for a certain ϵ_r and the value obtained for $\epsilon_r = 1$. The results show the applicability of flexible substrates (including paper) to permittivity detection.

The sensitivity (S) can be calculated as the variation of the first-notch frequency (Δf_r) divided by the variation of the relative permittivity ($\Delta\epsilon_r$), that is, $S = \Delta f_r/\Delta\epsilon_r$. By considering the relative variation of frequency expressed as a percentage [14], the relative sensitivity can be defined: $S_f = (100 \times \Delta f_r/f_r)/\Delta\epsilon_r$. Table 4 summarizes the values obtained for S and S_f. Column labels $\epsilon_r = \epsilon_r^i, \epsilon_r^j$ mean that the values are obtained by considering the variation from ϵ_r^i to ϵ_r^j. If the variation of ϵ_r is from 1 to 4, the highest S_f value is achieved by Kapton, followed by Mitsubishi paper. Kodak paper, followed by LCP, shows the highest S_f value from $\epsilon_r = 4$ to $\epsilon_r = 7$. The largest value for changes of ϵ_r from 7 to 10 and from 10 to 20 is achieved by LCP substrate.

Table 4: Sensitivity (S (MHz)) and relative sensitivity (S_f (%)).

	$\epsilon_r = 1, 4$		$\epsilon_r = 4, 7$		$\epsilon_r = 7, 10$		$\epsilon_r = 10, 20$	
	S	S_f	S	S_f	S	S_f	S	S_f
FR4	31	3.2	20	2.3	15	1.8	9	1.2
RO4003C	37	3.8	22	2.6	17	2.1	9	1.2
I-Tera	18	1.9	15	1.7	8	1.0	4	0.5
Kapton	45	4.6	25	2.9	19	2.4	12	1.6
LCP	35	3.7	24	3.0	19	2.5	12	1.7
Mitsubishi	41	4.0	22	2.4	20	2.3	11	1.4
Kodak	37	3.9	28	3.3	15	2.0	10	1.3

4.2. Experimental validation of RO4003C prototype with low-loss MUTs

An experimental test using samples of dielectric materials with low permittivity tolerance has been performed. The materials are: polycarbonate (PC), polypropylene (PP) and polystyrene (PS). Their reference permittivity values have been taken from the literature. The frequency shifts in S_{11} first notch achieved when the MUT is placed on the sensor with respect to the results without the MUT are measured with a network analyzer. Using the results of S obtained by full-wave EM simulation, shown in Table 4, and the measured frequency shift $\Delta f_{r,meas}$, the permittivity value can be estimated from the measurements as $\epsilon_r = 1 + \Delta f_{r,meas}/S$. The results are shown in Table 5. All the considered MUTs are low-loss materials, with values of tanδ below 0.0001 at room temperature.

Table 5: Relative permittivity of different common plastic MUTs.

	Reference ϵ_r	$\Delta f_{r,meas}$ (MHz)	ϵ_r estimated from measurements
PC	2.75-2.81 at 10 GHz [40]	60.0	2.62
PP	2.25 at 1 GHz [41]	45.5	2.23
PS	2.50-2.60 at 10.7 GHz [40]	60.0	2.62

In the case of PP, material for which the reference value at 1 GHz is provided in the cited work, the relative error between the MUT ϵ_r value estimated from the measurements and the reference value is 0.89%. The extracted permittivity value depends on the reflection measurements (S_{11}), performed to determine $\Delta f_{r,meas}$, and the EM simulations that have led to the estimation of the sensitivity. Both the S-parameter measurements and the numerical simulations are subject to uncertainty. S-parameter measurements are performed with a vector network analyzer. After a full two-port calibration has removed systematic errors, the instrumentation error can be considered negligible in comparison to the uncertainty components related to the EM simulations.

The most relevant sources of uncertainty affecting these numerical simulations are the tolerances of the laminate parameters. Simulations have been performed to quantify the effect of these tolerances. CST Microwave studio has been used to check the effect of a variation of RO4003C substrate thickness within the tolerance range specified by the manufacturer ($\pm 0.002''$). By considering this variation, extracted ϵ_r values in the range 1.90-2.25 have been obtained. Also, CST simulations have been run by considering variations of the relative permittivity of the substrate within a ± 0.05 tolerance. The impact of this tolerance is lower. The MUT ϵ_r value extracted from the measured $\Delta f_{r,meas}$ varies in the range 2.20-2.25.

4.3. Substrate-dependent analysis based on simulations with lossy MUTs

In subsection 4.1, for simplicity the MUT is assumed to be lossless. The experimental validation shown in subsection 4.2 is based on low-loss MUTs. The next step is to analyze the performance of the proposed type of sensor in the case of MUTs with higher losses. To achieve this goal, a simulation example in the context of soil moisture sensing is shown.

CST includes two pre-defined "soil" materials. One of them corresponds to a dry soil ($\epsilon_r = 2.55$, $\tan \delta = 0.0014$) and the other one to a wet loamy soil with 13.77% moisture ($\epsilon_r = 13.8$, $\tan \delta = 0.18$). These materials have been used to define MUTs. In both cases, MUT losses have been taken into account.

EM simulations have been performed using the sensors based on RO4003C, Ultralam 3850 LCP and Mitsubishi photo-paper in contact with the MUTs. Fig. 7 presents the reflection parameters S_{11} versus frequency. In the case of paper, for wet soil the first notch is located near 0.6 GHz. However, there is an upper notch, close to 1 GHz, which is near the first notch for dry soil (at 0.94 GHz). This proximity, together with the low Q factor, increases the risk of failure in moisture detection. This behavior is not observed with RO4003C and Ultralam 3850 LCP substrates. In both cases, the upper notches for wet soil are clearly separated from the first notch for dry soil.

5. Impact of bending on resonator performance

In contrast to rigid substrates, flexible laminates allow to bend a PCB for a better adaptation to a variety of surfaces. Full-wave EM simulations have been run to investigate the impact of bending on the performance of the planar sensors. For this purpose, the 3D EM models of the resonators in CST have been bent, as it is shown in Fig. 8. These 3D models are parameterized. The parameter θ_{deg} ranges from 0 to 120°, and it represents the angle or arc formed by bending the resonator (with length L_{PCB} in the bending dimension) over a cylinder with radius R. Thus, $L_{PCB} = R\theta_{rad}$, where θ_{rad} is the angle expressed in radians. For a bending angle of 120°, the sensors could be placed in contact to cylindrical shapes of radius in the range 6.6-7.8 cm.

The performance of the sensor is analyzed for different bending conditions. Figs. 9 and 10 show the variation of the first-notch frequency versus the bending angle, for different values of MUT relative permittivity. Table 6 shows the maximum percentage variation of this specific frequency due to bending for the considered angle range. It can be observed that the variations are within the range 0.4% - 4.7%.

Table 6: Maximum percentage variation of first-notch frequency due to bending for θ_{deg} ranging from 0 to 120°.

	Ultralam 3850-LCP	Kapton 500 HN	Mitsubishi paper	Kodak paper
$\epsilon_r = 1$	0.50%	2.16%	1.52%	4.74%
$\epsilon_r = 4$	1.09%	0.45%	0.40%	2.71%
$\epsilon_r = 7$	0.49%	0.56%	2.31%	2.52%
$\epsilon_r = 10$	0.84%	0.98%	2.36%	2.08%
$\epsilon_r = 20$	1.83%	2.16%	4.62%	3.17%

6. Discussion

Future IoT applications demand that sensor development is focused not only on performance aspects, such as high sensitivity, but also on cost and sustainability. Therefore, low-cost, environmentally-friendly materials and manufacturing processes should be the preferred choice. In comparison to subtractive techniques, inkjet printing allows to reduce by-products, such as strong acids (wet etching) or metal dust (milling machines).

Different substrates are available that show flexibility (to match non-flat geometries) and allow inkjet printing. LCP and paper are sustainable options. Paper substrates are, also, ultra low-cost. A general drawback for the development of high-frequency circuits based on paper substrates is the high dielectric loss. However, there are applications that can afford this drawback and it is possible to find contributions in the scientific literature that present PCB circuits and patch antennas on this type of substrates [42, 43].

This article has explored the potential of paper substrates in comparison to other ones to implement a microstrip sensor for permittivity detection in reflection mode. The layout geometry has been selected due to its easy manufacturing, since it does not include elements (in-line gaps, narrow slots or via-holes) that could be critically affected by manufacturing tolerances, so that even inkjet printing with an office printer could be used to produce them. Al-

though the performance of this simple structure is limited in terms of Q-factor, the frequency shift and notch depth of the reflection response allow its use for ultra-low cost applications in which only coarse differences in permittivity are required. For example, these flexible sensors may be useful to establish conservative risk thresholds regarding the structural health of timber or concrete structures.

Two simulation scenarios have been considered regarding losses: lossless (Figs. 4 and 5) and lossy MUTs (soil example, Fig. 7). In the example about soil, with paper substrate the curve for dry soil is similar to the curve for the lossless MUT case (Fig. 5). The MUT losses in this case are low ($\tan\delta = 0.0014$ for dry soil). However, for wet soil ($\tan\delta = 0.18$) the second local minimum of S_{11} is very close to the first-notch for dry soil and there is an important notch depth reduction. This behavior is not observed in the case of LCP or Rogers substrates. In the case of paper, the combined effect of high substrate losses and high MUT losses leads to a higher risk of detection failure. It can be concluded that the problems arise when considering MUTs with high losses together with lossy substrates. Therefore the applicability of this sensor on paper substrate must be restricted to low-loss MUTs, whereas LCP is applicable to a wider range of MUTs. Applications with realistic low-loss MUTs and lower frequencies on paper substrates will be tested in future work. For example, drying processes involving removal of water are characterized by a decrease of ϵ_r and often by a decrease of dielectric loss. Therefore, a potential application scenario for this type of paper-based sensors might be ultra-low cost monitoring of drying processes at final stage.

The analysis of the impact of bending on the first-notch frequency provides values between 0.4% and 4.7%. These values should be considered in comparison to the variations due to changes in the relative permittivity of the MUT shown in Fig. 6. For example, by using the Mitsubishi paper substrate the variation of resonance frequency produced by a change in ϵ_r from 1 to 4 is 0.12 (12%), whereas the variations due to bending for $\epsilon_r = 1$ and $\epsilon_r = 4$ are 1.5% and 0.4%. These variations due to bending should not be neglected if the sensor

is aimed at detecting 12% variations due to MUT permittivity. Therefore, a custom calibration for a concrete task with a specific bending angle should be performed for an accurate measurement if the whole structure is intended to be bent. It is also possible to use the structure with the bent substrate pressed against the MUT, flattening the contact area while leaving the feeding bent.

The experimental validation of the sensor concept on the available substrate (RO4003C) has shown that it can be used to perform estimations of permittivity in the case of reference common plastic materials. This prototype can also be used in the lab as a 1-GHz low-cost permittivity probe for other materials with unknown relative permittivity. A performance comparison with previous work on state-of-the-art microwave planar sensors for permittivity measurements is shown in Table 7, where f_0 represents the reference operating frequency. The specified figures of merit (FoMs) correspond to measured values, unless it is otherwise indicated in the last column. In the case of several MUTs measured [8, 9, 19], S and S_f are average values calculated from the different measurements.

7. Conclusion

Green electronics is meant to play a dominant role in the IoT era to avoid a huge, unsustainable increase in electronic waste due to the spread of sensors. Microwave sensors constitute an attractive technology that allows to perform real-time material characterization in a non-invasive way. Therefore, eco-friendly microwave sensing should become one of the key technologies in the next-generation IoT context.

The presented results demonstrate that it is possible to obtain resonator-based sensors on PCB technology by using environmentally-friendly substrate materials such as LCP or paper. Paper-based substrates, which have the advantages of being ultra low-cost and biodegradable, can be considered in applications involving low-loss MUTs. LCP has shown its potential also for lossy MUTs. The results can serve as a design roadmap towards low-cost and sustainable planar resonator sensors for real-time monitoring of permittivity.

Table 7: Performance of various microwave planar sensors for dielectric characterization of solid or liquid materials. Measured values, unless otherwise indicated.

Ref.	f_0 (GHz)	S (MHz)	S_f (%)	ϵ_r range measured or other FoMs
[5]	1.6	N/A	N/A	2.2×10^{-3} dB change in S_{11} for 0.1 mg/L change of Zn concentration
[8]	2.7	111.1	4.1	Solid MUTs, ϵ_r measured: 1-10.2
[9]	2.5	15.7	0.6	Solid MUTs, ϵ_r measured: 1-6.7
[14]	0.9	0.8	0.9	Measured using water/ethanol solutions
[15]	19.4	N/A	N/A	-0.085 dB/vol.%, IPA-water (0-100 vol.%) 0.00023 dB/[mg/dL], glucose solution 0.00056 dB/[mg/dL], NaCl solution
[16]	4.0	13.0	3.3	Experimental validation in air
[19]	1.9	N/A	5.0	Solid MUTs, ϵ_r measured: 1-9.8
[20]	2.8	N/A	N/A	Sim: freq. shift $>$ 30 MHz, amplitude change $>$ 30 dB for strain range 0.6-21.3% Experimental validation: 0.6-10% strain
This work	1.0	36.4	3.6	Solid MUTs, ϵ_r measured: 1-2.25

Further work should focus on planar resonator geometries on flexible biodegradable substrates optimized to improve sensitivity and on calibration for specific tasks in the multiple areas where they find application. Also, sustainable conductive materials should be a major topic of research to produce truly green microwave sensors at an affordable price.

8. Acknowledgments

The authors would like to thank Mr. V. Kilaru for measurements and Mr. A. Gómez for useful discussions. This research has been supported by Ministerio de Educación y Formación Profesional (Collaboration Grant at the De-

partment of Computer and Communication Technologies), the European Union (ERASMUS + Programme, Mobility for Traineeship), project TEC2017-83352-C2-2-P (Agencia Estatal de Investigación) and project GR18055 (Junta de Extremadura/European Regional Development Funds, EU).

References

[1] L. Crocco, P. Kosmas, Electromagnetic technologies for medical diagnostics: fundamental issues, Clinical Applications and Perspectives, MDPI, 2019.

[2] M. Malajner, D. Gleich, P. Planinsic, Soil type characterization for moisture estimation using machine learning and UWB-time of flight measurements, Measurement 146 (2019) 537–543.

[3] J. A. T. Vasquez, R. Scapaticci, G. Turvani, M. Ricci, L. Farina, A. Litman, M. R. Casu, L. Crocco, F. Vipiana, Noninvasive inline food inspection via microwave imaging technology: An application example in the food industry, IEEE Antennas and Propagation Magazine 62 (5) (2020) 18–32.

[4] V. Guihard, F. Taillade, J.-P. Balayssac, B. Steck, J. Sanahuja, F. Deby, Permittivity measurement of cementitious materials with an open-ended coaxial probe, Construction and Building Materials 230 (2020) 116946.

[5] I. Frau, S. Wylie, P. Byrne, J. Cullen, O. Korostynska, A. Mason, Detection of Zn in water using novel functionalised planar microwave sensors, Materials Science and Engineering: B 247 (2019) 114382.

[6] I. Yaroshenko, D. Kirsanov, M. Marjanovic, P. A. Lieberzeit, O. Korostynska, A. Mason, I. Frau, A. Legin, Real-time water quality monitoring with chemical sensors, Sensors 20 (12) (2020) 3432.

[7] K. Y. You, C. Y. Lee, Y. L. Then, S. H. C. Chong, L. L. You, Z. Abbas, E. M. Cheng, Precise moisture monitoring for various soil types us-

ing handheld microwave-sensor meter, IEEE Sensors Journal 13 (7) (2013) 2563–2570.

[8] C.-S. Lee, C.-L. Yang, Complementary split-ring resonators for measuring dielectric constants and loss tangents, IEEE Microwave and Wireless Components Letters 24 (8) (2014) 563–565.

[9] S. Subbaraj, V. S. Ramalingam, M. Kanagasabai, E. F. Sundarsingh, Y. P. Selvam, S. Kingsley, Electromagnetic nondestructive material characterization of dielectrics using EBG based planar transmission line sensor, IEEE Sensors Journal 16 (19) (2016) 7081–7087.

[10] J. Nehring, M. Schütz, M. Dietz, I. Nasr, K. Aufinger, R. Weigel, D. Kissinger, Highly integrated 4–32-GHz two-port vector network analyzers for instrumentation and biomedical applications, IEEE Transactions on Microwave Theory and Techniques 65 (1) (2016) 229–244.

[11] R. Mirzavand, M. M. Honari, P. Mousavi, High-resolution dielectric sensor based on injection-locked oscillators, IEEE Sensors Journal 18 (1) (2017) 141–148.

[12] S. Lim, C.-Y. Kim, S. Hong, Simultaneous measurement of thickness and permittivity by means of the resonant frequency fitting of a microstrip line ring resonator, IEEE Microwave and Wireless Components Letters 28 (6) (2018) 539–541.

[13] K. M. Shafi, A. K. Jha, M. J. Akhtar, Improved planar resonant RF sensor for retrieval of permittivity and permeability of materials, IEEE Sensors Journal 17 (17) (2017) 5479–5486.

[14] P. Vélez, L. Su, K. Grenier, J. Mata-Contreras, D. Dubuc, F. Martín, Microwave microfluidic sensor based on a microstrip splitter/combiner configuration and split ring resonators (SRRs) for dielectric characterization of liquids, IEEE Sensors Journal 17 (20) (2017) 6589–6598.

[15] S. Mohammadi, B. Wiltshire, M. C. Jain, A. V. Nadaraja, A. Clements, K. Golovin, D. J. Roberts, T. Johnson, I. Foulds, M. H. Zarifi, Gold coplanar waveguide resonator integrated with a microfluidic channel for aqueous dielectric detection, IEEE Sensors Journal 20 (17) (2020) 9825–9833.

[16] M. Amirian, G. Karimi, B. D. Wiltshire, M. H. Zarifi, Differential narrow bandpass microstrip filter design for material and liquid purity interrogation, IEEE Sensors Journal 19 (22) (2019) 10545–10553.

[17] M. H. Zarifi, S. Deif, M. Abdolrazzaghi, B. Chen, D. Ramsawak, M. Amyotte, N. Vahabisani, Z. Hashisho, W. Chen, M. Daneshmand, A microwave ring resonator sensor for early detection of breaches in pipeline coatings, IEEE Transactions on Industrial Electronics 65 (2) (2018) 1626–1635.

[18] S. A. Alotaibi, Y. Cui, M. M. Tentzeris, CSRR based sensors for relative permittivity measurement with improved and uniform sensitivity throughout [0.9-10.9] GHz band, IEEE Sensors Journal 20 (9) (2020) 4667–4678.

[19] L. Su, X. Huang, W. Guo, H. Wu, A flexible microwave sensor based on complementary spiral resonator for material dielectric characterization, IEEE Sensors Journal 20 (4) (2020) 1893–1903.

[20] Z. A. Dijvejin, K. K. Kazemi, K. Alasvand Zarasvand, M. H. Zarifi, K. Golovin, Kirigami-enabled microwave resonator arrays for wireless, flexible, passive strain sensing, ACS Applied Materials & Interfaces 12 (39) (2020) 44256–44264.

[21] H. Hallil, P. Bahoumina, K. Pieper, J. L. Lachaud, D. Rebière, A. Abdelghani, K. Frigui, S. Bila, D. Baillargeat, Q. Zhang, et al., Differential passive microwave planar resonator-based sensor for chemical particle detection in polluted environments, IEEE Sensors Journal 19 (4) (2019) 1346–1353.

[22] Y. Morimoto, M. Memarian, X. Li, T. Itoh, Open-end microstrip line ter-

minations using lossy gray-scale inkjet printing, IEEE Transactions on Microwave Theory and Techniques 65 (12) (2017) 4861–4870.

[23] C. Beisteiner, B. Zagar, An inkjet-printed ambient RF energy harvester, Proceedings Sensor 2017 (2017) 546–550.

[24] C. Baytöre, E. Y. Zoral, C. Göçen, M. Palandöken, A. Kaya, Coplanar flexible antenna design using conductive silver nano ink on paper substrate for wearable antenna applications, in: 2018 28th International Conference Radioelektronika (RADIOELEKTRONIKA), IEEE, 2018, pp. 1–6.

[25] B. Sanz-Izquierdo, S. Jun, J. Heirons, N. Acharya, Inkjet printed and folded LTE antenna for vehicular application, in: 2016 46th European Microwave Conference (EuMC), IEEE, 2016, pp. 88–91.

[26] F. B. Ashraf, T. Alam, M. T. Islam, A printed xi-shaped left-handed metamaterial on low-cost flexible photo paper, Materials 10 (7) (2017) 752.

[27] S. Sivapurapu, R. Chen, C. Mehta, Y. Zhou, M. L. Bellaredj, X. Jia, P. A. Kohl, T.-C. Huang, S. K. Sitaraman, M. Swaminathan, Multi-physics modeling and characterization of components on flexible substrates, IEEE Transactions on Components, Packaging and Manufacturing Technology 9 (9) (2019) 1730–1740.

[28] R. Awang, Flexible and tunable split ring resonators, Ph.D. thesis, School of Electrical and Computer Engineering, RMIT University (2016).

[29] W. Li, Y. Hei, P. M. Grubb, X. Shi, R. T. Chen, Compact inkjet-printed flexible MIMO antenna for UWB applications, IEEE Access 6 (2018) 50290–50297.

[30] S. Amendola, A. Palombi, G. Marrocco, Inkjet printing of epidermal RFID antennas by self-sintering conductive ink, IEEE Transactions on Microwave Theory and Techniques 66 (3) (2018) 1561–1569.

[31] J. Kimionis, S. Shahramian, Y. Baeyens, A. Singh, M. M. Tentzeris, Pushing inkjet printing to W-band: An all-printed 90-GHz beamforming array, in: 2018 IEEE/MTT-S International Microwave Symposium-IMS, IEEE, 2018, pp. 63–66.

[32] F. Mokhtari-Koushyar, P. M. Grubb, M. Y. Chen, R. T. Chen, A miniaturized tree-shaped fractal antenna printed on a flexible substrate: A lightweight and low-profile candidate with a small footprint for spaceborne and wearable applications, IEEE Antennas and Propagation Magazine 61 (3) (2019) 60–66.

[33] Y. Lan, Y. Xu, C. Wang, Z. Wen, Y. Qiu, T. Mei, Y. Wu, R. Xu, X-band flexible bandpass filter based on ultra-thin liquid crystal polymer substrate, Electronics Letters 51 (4) (2015) 345–347.

[34] R. Moro, S. Kim, M. Bozzi, M. Tentzeris, Inkjet-printed paper-based substrate-integrated waveguide (SIW) components and antennas, International Journal of Microwave and Wireless Technologies 5 (3) (2013) 197–204.

[35] M. Poggiani, F. Alimenti, P. Mezzanotte, M. Virili, C. Mariotti, G. Orecchini, L. Roselli, 24-GHz patch antenna array on cellulose-based materials for green wireless internet applications, IET Science, Measurement & Technology 8 (6) (2014) 342–349.

[36] C. Mariotti, F. Alimenti, L. Roselli, M. M. Tentzeris, High-performance RF devices and components on flexible cellulose substrate by vertically integrated additive manufacturing technologies, IEEE Transactions on Microwave Theory and Techniques 65 (1) (2017) 62–71.

[37] H. Saghlatoon, L. Sydänheimo, L. Ukkonen, M. Tentzeris, Optimization of inkjet printing of patch antennas on low-cost fibrous substrates, IEEE Antennas and wireless propagation letters 13 (2014) 915–918.

[38] R. R. Mohan, B. Paul, S. Mridula, P. Mohanan, Measurement of soil moisture content at microwave frequencies, Procedia Computer Science 46 (2015) 1238–1245.

[39] V. Komarov, S. Wang, J. Tang, Permittivity and measurements, Encyclopedia of RF and microwave engineering.

[40] B. Riddle, J. Baker-Jarvis, J. Krupka, Complex permittivity measurements of common plastics over variable temperatures, IEEE Transactions on Microwave Theory and Techniques 51 (3) (2003) 727–733.

[41] T. C. Edwards, M. B. Steer, Foundations for microstrip circuit design, John Wiley & Sons, 2016.

[42] S. Moscato, N. Delmonte, L. Silvestri, M. Pasian, M. Bozzi, L. Perregrini, Compact substrate integrated waveguide (SIW) components on paper substrate, in: 2015 European Microwave Conference (EuMC), IEEE, 2015, pp. 24–27.

[43] H. F. Abutarboush, A. Shamim, A reconfigurable inkjet-printed antenna on paper substrate for wireless applications, IEEE Antennas and Wireless Propagation Letters 17 (9) (2018) 1648–1651.

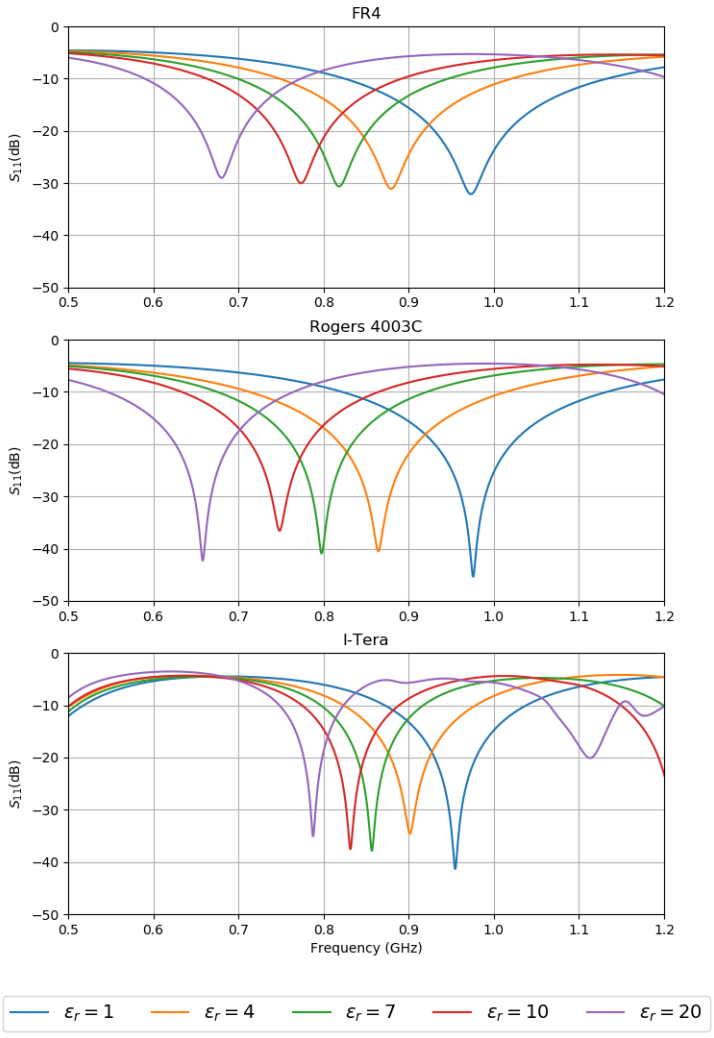

Figure 4: Impact of MUT relative permittivity on the reflection performance of the structure, for different rigid substrates.

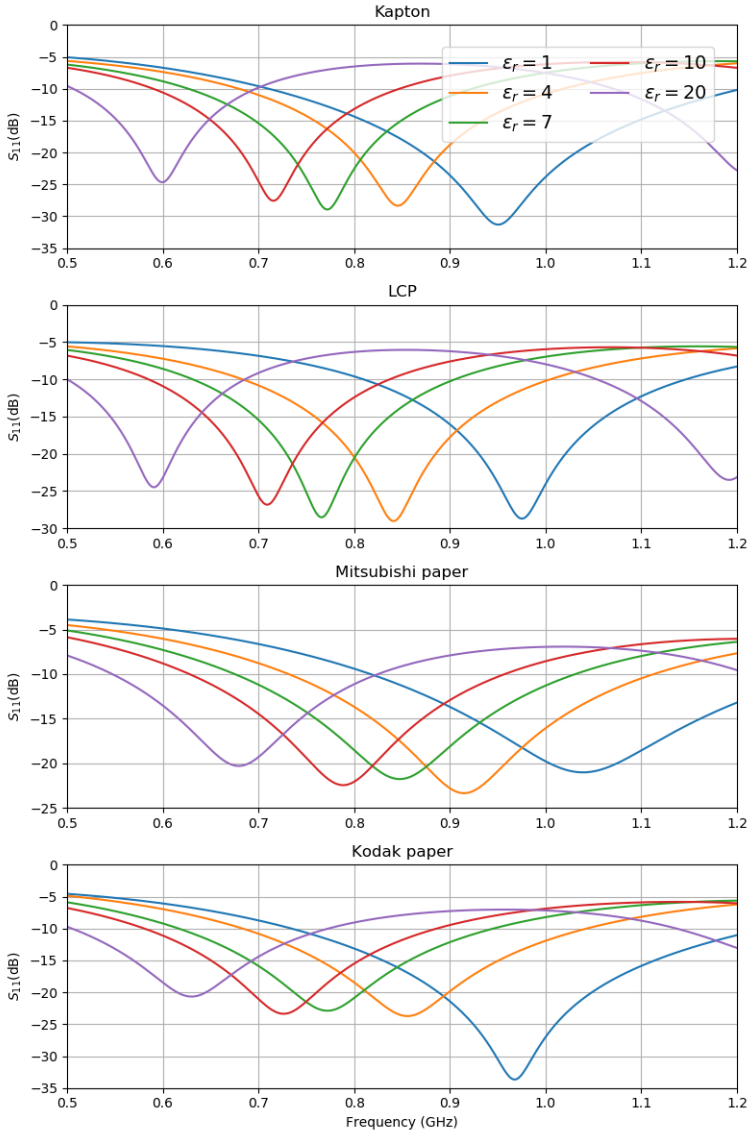

Figure 5: Impact of MUT relative permittivity on the reflection performance of the structure, for different flexible substrates.

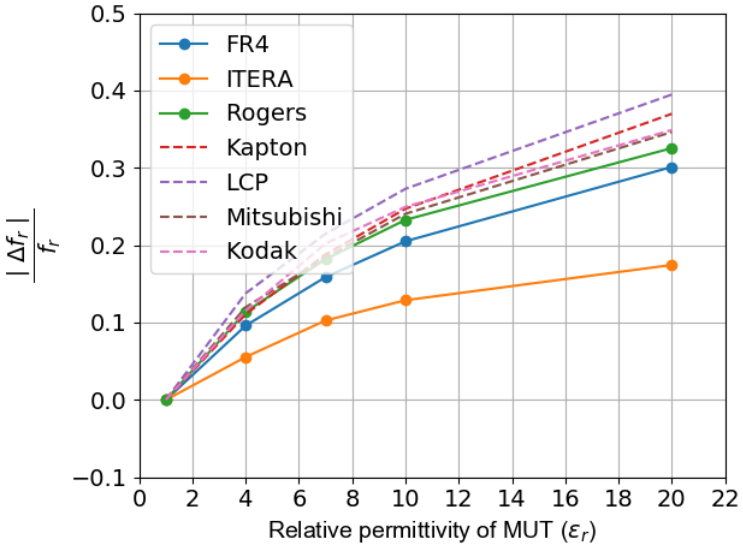

Figure 6: Relative variation of resonance frequency with respect to the value for $\epsilon_r = 1$ versus MUT relative permittivity. Dashed (solid) lines refer to flexible (rigid) substrates.

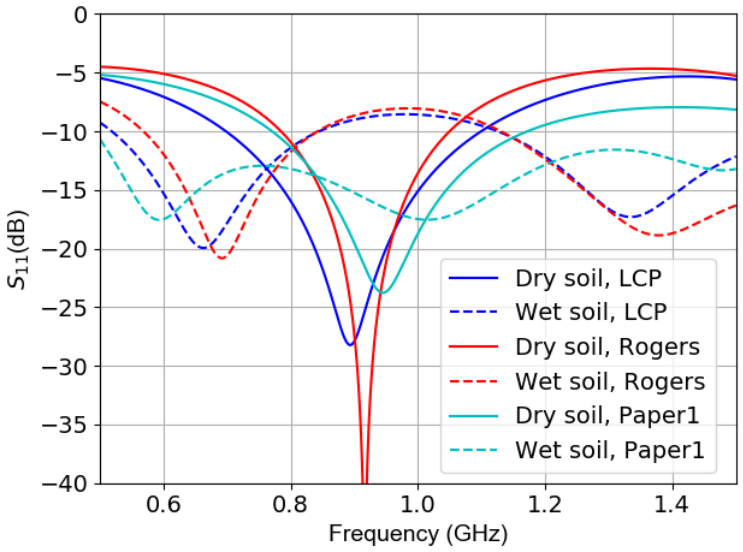

Figure 7: Reflection parameter of the sensor versus frequency for two soil-type MUTs and different substrates. Results obtained using EM simulations.

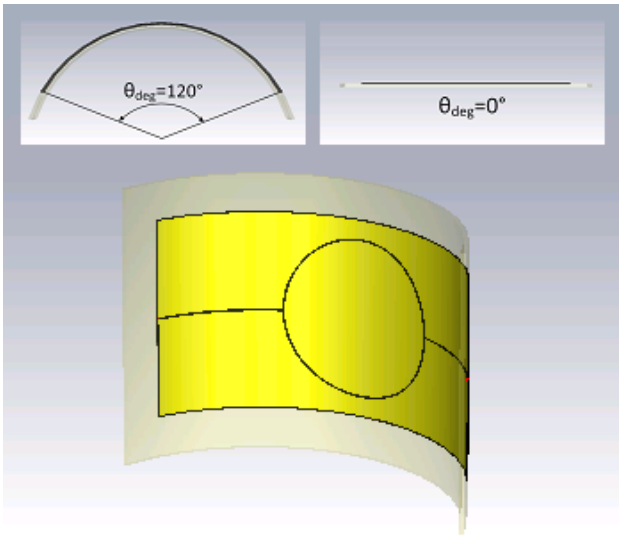

Figure 8: 3D model of a bent structure.

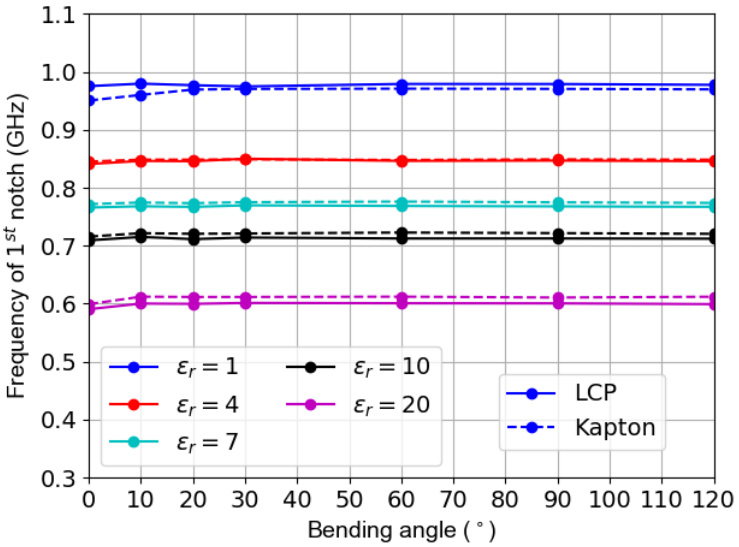

Figure 9: Variation of resonance frequency versus bending angle, for different permittivity values of the MUT, using LCP and Kapton substrates. Results obtained using full-wave EM simulations.

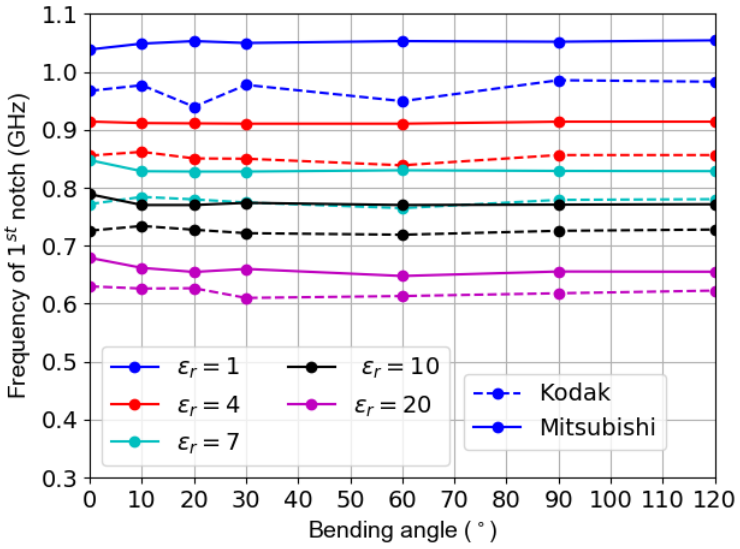

Figure 10: Variation of resonance frequency versus bending angle, for different permittivity values of the MUT, using paper (Mitsubishi and Kodak) substrates. Results obtained using full-wave EM simulations.